Journal of
Nanoscience and Nanotechnology
Vol. 9, 2677–2681, 2009

Improved Upconversion Luminescence Properties of $Gd_2O_3:Er^{3+}/Gd_2O_3:Yb^{3+}$ Core–Shell Nanorods

Xue Bai[1], Hongwei Song[1,*], Guohui Pan[2], Xinguang Ren[2], Biao Dong[1], Qilin Dai[2], and Libo Fan[2]

[1] *State Key Laboratory on Integrated Optoelectronics, College of Electronic Science and Engineering, Jilin University, Changchun 130012, P. R. China*
[2] *Key Laboratory of Excited State Physics, Changchun Institute of Optics, Fine Mechanics and Physics, Chinese Academy of Sciences, Changchun 130033, People's Republic of China and The Graduate School of Chinese Academy of Sciences, Changchun 130033, People's Republic of China*

The $Gd_2O_3:Er^{3+}/Gd_2O_3:Yb^{3+}$ core–shell nanorods (NRs) as well as Er^{3+} and Yb^{3+} homogeneously codoped Gd_2O_3 NRs were synthesized by the hydrothermal method. The average diameters of the NRs are ~20 nm and the lengths are 150–200 nm. The thickness of the $Gd_2O_3:Yb^{3+}$ shells on the $Gd_2O_3:Er^{3+}$ cores are ~5 nm. The upconversion luminescence (UCL) properties of the core–shell NRs have been studied in contrast to homogeneously codoped NRs under 978-nm laser diode excitation. Green emissions of $^2H_{11/2}$, $^4S_{3/2}$–$^4I_{15/2}$, and red emissions of $^4F_{9/2}$–$^4I_{15/2}$ were observed. Relative intensity of the red ($^4F_{9/2}$–$^4I_{15/2}$) to the green ($^4S_{3/2}$/$^2H_{11/2}$–$^4I_{15/2}$) and the intensity ratio (R_{HS}) of $^2H_{11/2}$–$^4I_{15/2}$ to $^2H_{11/2}$–$^4I_{15/2}$ decrease obviously in the core–shell NRs compared to the NRs. The power-dependence of UCL intensity and the thermal effect caused by 978-nm diode laser irradiation was studied. The result indicates that the cross-relaxation effect and the thermal effect in the core–shell structure is effectively depressed.

Keywords: Lanthanide, Photoluminescence, Nanocrystals.

RESEARCH ARTICLE

1. INTRODUCTION

Recently, one-dimensional (1D) rare earth ions doped nanophosphors have received extensive attention due to their potential application in fields such as optoelectronic devices,[1,2] low-threshold laser,[3] biological fluorescence labels etc.[4,5] 1D core–shell composite structures are extensive scientific and technological interests due to the ability to tune their properties.[6–8] Core–shell materials consist of a core structural domain covered by a shell domain. In this structure, on one hand, the surface defects around the luminescent ions can be modified, thus reducing the nonradiative pathways. On the other hand, the core's properties can be influenced by the surface addition of selected atomic or molecular species. Up to now, many reports are available regarding ways to improve the luminescent characteristic of nanocrystals.[9–11]

Upconversion luminescence (UCL) from near-infrared (NIR) to visible wavelength in materials doped with trivalent rare earth (RE) ions has attracted considerable interests, especially since the availability of high-power infrared laser diodes.[12–13] As the candidates of upconversion nonmaterial Gd_2O_3 nanocrystals (NCs) doped with Er^{3+} ions and sensitized with Yb^{3+} ions has been widely studied due to Er^{3+} ion has a favorable energy levels capable of infrared pumping that closely matches the most attractive 978-nm laser diode (LD) wavelength, which is in fair agreement with the peak wavelength of Yb^{3+} ion absorption.[14] Increasing the Yb^{3+} concentration can result in increase UC efficiency. Nevertheless, too high dopant concentration will quench the UCL due to the cross relaxation. Our previous work has found that with increase of the Yb^{3+} concentration, the sample temperature at the irradiated spot increases remarkably, which will lead to the quenching of UCL.[14] Therefore, the dopant ions spatial distribution and the depressing of the thermal effect are expected to play the important roles in the UCL. Here, we prepared the $Gd_2O_3:Er^{3+}/Gd_2O_3:Yb^{3+}$ core–shell nanorods (NRs), which spatially separate the Er^{3+} and Yb^{3+} ions in two different layers. It is important to observe that separating the luminescent centers (Er^{3+}) from the Yb^{3+} ions can effectively reduce the local thermal effect induced by laser irradiation.

2. EXPERIMENTAL DETAILS

The samples were prepared by the two-step hydrothermal method. Synthesis of $Gd(OH)_3:Er^{3+}$(2%) core and

*Author to whom correspondence should be addressed.

 1533-4880/2009/9/2677/005 doi:10.1166/jnn.2009.1295

codoped $Gd_2O_3:Er^{3+}$, Yb^{3+}(2%, 2%) NRs:appropriate amounts of high purity Gd_2O_3, Er_2O_3 (1:0.02 mol ratio) and Gd_2O_3, Er_2O_3, Yb_2O_3 (1:0.02:0.02 mol ratio) were dissolved in concentrated HNO_3 first. Then appropriate volume dilute KOH solution was added to the nitrate solution to form $Gd(OH)_3$. Diluted KOH solution (1 M) was used to adjust the pH values of $Gd(OH)_3$ solutions; the final pH value was 13. After a thorough stirring, the colloid solution was transferred into several closed Teflon-lined autoclaves and subsequently heated to 130 °C for 17 h. The obtained suspension was centrifuged and supernatant was discarded. The resultant precipitate was washed with de-ionized water several times, and then the codoped $Gd(OH)_3$ precipitate was dried at 70 °C. Following the above procedure, the codoped $Gd(OH)_3$ powders were obtained and converted into $Gd_2O_3:Er^{3+}$, Yb^{3+} (2%, 2%) after annealing at 500 °C for 2 h. This sample is named NRs.

Coating of $Gd_2O_3:Er^{3+}$ (2%) core with $Gd_2O_3:Yb^{3+}$ (2%/4%) shells: the obtained $Gd(OH)_3:Er^{3+}$ (2%) core precipitate was divided into equal two parts on average. Appropriate amounts of $Gd(NO_3)_3$, $Yb(NO_3)_3$ (1:0.02/0.04 mol ratio) solution and the two core precipitate were mixed in molar ratio of 0.5:1, respectively. After ultrasonically dispersing for about 1 h, ammonia solution (0.2 M) was slowly added, and the final pH value was adjusted to 10–11. The as-obtained colloidal precipitate was transferred into several autoclaves and kept at 170 °C for 17 h. The precipitate was then centrifuged, washed, dried and annealed at 500 °C for 2 h. In this way, the core–shell structured $Gd_2O_3:Er^{3+}$ (2%)/$Gd_2O_3:Yb^{3+}$ (2%) and $Gd_2O_3:Er^{3+}$ (2%)/$Gd_2O_3:Yb^{3+}$ (4%) core–shell NRs have been obtained. The samples are named as CS1 and CS2, respectively.

In the measurements, X-ray diffraction (XRD) data were collected on Rigaku/max-rA X-ray diffractometer using a Cu target radiation source ($\lambda = 1.54078$ Å). Transmission electron micrographs (TEM) were taken on JEM-2010 electron microscope. High-resolution transmission electron micrographs (HR-TEM) images were recorded on a JEM-3010 transmission electron microscope. In UCL experiments, a 978-nm diode laser having a powder maximum of 2 W was used to pump the samples. The visible emissions were collected using a Hitachi F-4500 spectrophotometer equipped with a continuous 150 W Xe-arc lamp.

3. RESULTS AND DISCUSSION

Figure 1(a) shows transmission electron microscopy (TEM) images of the nanocrystalline $Gd(OH)_3:Er^{3+}/Yb^{3+}$ powders before coating. It is obvious that all the nanocrystalline powders yield homogeneous NRs, with

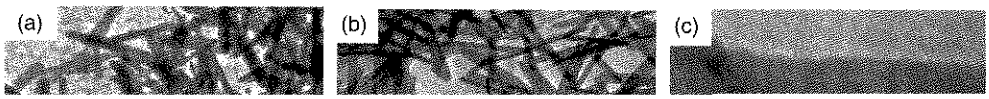

average diameter of ~20 nm and length of 150–200 nm. Figure 1(b) gives the TEM image of the dehydration of the $Gd(OH)_3:Er^{3+}/Yb^{3+}$ NRs. We can see that the morphologies of these nanostructures could be maintained after thermal treatment and the sizes of the Gd_2O_3 NRs are slightly small than the hydroxide precursors owing to the elimination of H_2O in the calcinations process, which had been reported by some works.[15, 16] Some groups investigated the formation mechanism of growth of 1-D nanostructures.[16–18] They believed that the crystal structure is the important factor determines the growth behavior of the nanocrystals. As is well known, $Gd(OH)_3$ have a hexagonal crystal structure that is very preferable for the growth of NRs.[16] Figure 1(c) depicts the magnified image of the NRs shown in Figure 1(b), which demonstates that the surfaces of NRs are smooth and without amorphous layers. Figures 1(d) and (e) are the TEM images of the $Gd(OH)_3:Er^{3+}/Gd(OH)_3:Yb^{3+}$ and $Gd_2O_3:Er^{3+}/Gd_2O_3:Yb^{3+}$ NRs respectively. The Figure 1(f) displays a typical $Gd_2O_3:Er^{3+}/Gd_2O_3:Yb^{3+}$ NRs found in the composite. It can be observed that for most of the NRs the outer sides have been fully coated by $Gd_2O_3:Yb^{3+}$ layers. Figure 1(f) more clearly shows that the thickness of the coated outer-layer is usually ~5 nm, which can be identified by the brighter edge. The HRTEM image of an individual core–shell NRs shows that the core of Gd_2O_3 are well-crystallized and the multicrystal nature (Fig. 1(g)). The shell exhibits the crystallized layers closely adherent to the NRs surface. The innermost shell layers are approximately parallel to the growth axis of the core, while the outermost shell layers exhibit a somewhat disordered structure. Figure 2 shows the XRD patterns of the two different samples. It can be identified that the crystal structures of them all belong to pure cubic phase.

Figure 3 shows the normalized UCL spectra in Gd_2O_3 powders under 978-nm excitation in various samples. In the spectra the green lines of $^2H_{11/2}$, $^4S_{3/2}$–$^4I_{15/2}$ and red lines of $^4F_{9/2}$–$^4I_{15/2}$ can be distinguished. In comparison to the Er^{3+}, Yb^{3+} homogeneously doped Gd_2O_3 NRs, the

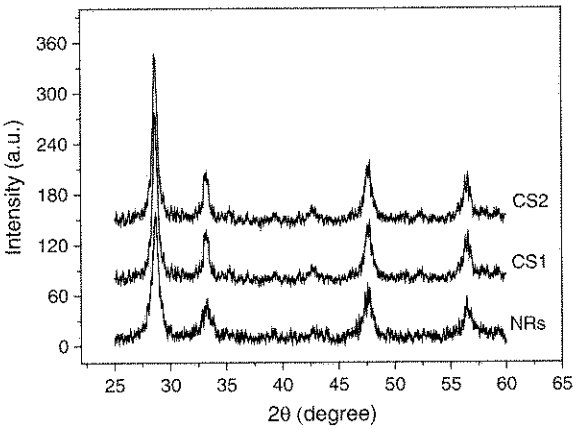

Fig. 2. The XRD patterns of the different powders.

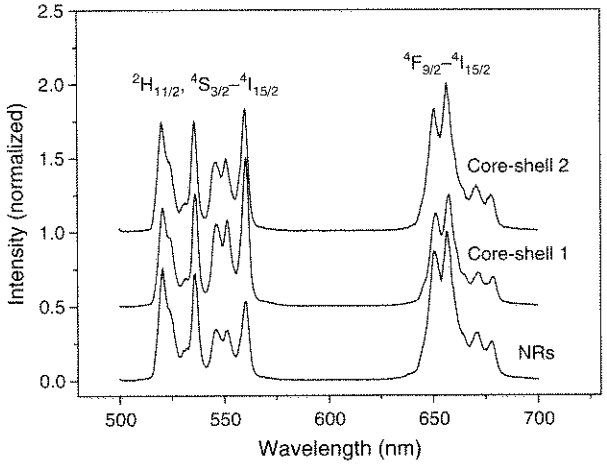

Fig. 3. Upconversion luminescent spectra in $Gd_2O_3:Er^{3+}/Yb^{3+}$ NRs and $Gd_2O_3:Er^{3+}/Gd_2O_3:Yb^{3+}$ core–shell NCs under 978-nm excitation (I_P = 752 mw).

UCL in the core–shell NRs demonstrate two features: (1) the relative intensity of the red ($^4F_{9/2}$–$^4I_{15/2}$) to the green ($^4S_{3/2}$/$^2H_{11/2}$–$^4I_{15/2}$) decreases; (2) and the intensity ratio (R_{HS}) of $^2H_{11/2}$–$^4I_{15/2}$ to $^2S_{3/2}$–$^4I_{15/2}$ decreases. The upconversion mechanism and population processes in Er^{3+} and Yb^{3+} codoped systems is well known, which were presented in Figure 4. The red and green upconversion occurs via two successive transfers of energy from theYb^{3+} ion to the Er^{3+} ion.[13, 14]: First, the Er^{3+} ions are exited from the ground state $^4I_{15/2}$ to the excited state $^4I_{11/2}$ via ET of neighboring Yb^{3+} and Er^{3+}. Subsequent nonradiative relaxations of $^4I_{11/2}$–$^4I_{13/2}$ also populate the $^4I_{13/2}$ level. Second, the same laser pumps the excited state ions from

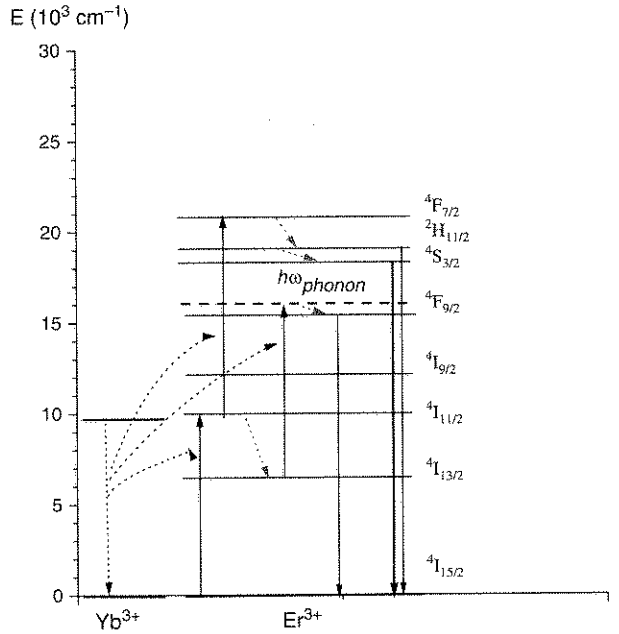

Fig. 4. The upconversion mechanism and population processes in Er^{3+} and Yb^{3+} codoped systems.

RESEARCH ARTICLE

the $^4I_{11/2}$ to the $^4F_{7/2}$ levels via ET and existed absorption (ESA), or from the $^4I_{13/2}$ to $^4F_{9/2}$ states via phonon-assisted ET. The excited ions on $^4F_{7/2}$ nonradiatively relax to the green levels of $^4S_{3/2}$ and $^2H_{11/2}$, generating green emission of $^4S_{3/2}$–$^4I_{15/2}$, while the excited Er^{3+} ions on $^4F_{9/2}$ generate red emission of $^4F_{9/2}$–$^4I_{15/2}$.

The relative intensity change of green to the red between the NRs and the core–shell NRs can be mainly attributed to the depressed nanradiative relaxation and the cross-relaxation process.[19] For the red emission, the nonradiative relaxation of $^4I_{11/2} \rightarrow {}^4I_{13/2}$ or the $^4F_{7/2} + {}^4I_{11/2} \rightarrow {}^4F_{9/2} + {}^4F_{9/2}$ cross-relaxation mechanism should be considered. In the NRs, the existence of surface contamination with available large vibrational modes such as CO_3^{2-} and OH^- leads the nonradiative relaxation to increase considerably. In the core–shell NRs, the surface of core is modified well by the shell. Thus, the nonradiative relaxation decreased due to those Er^{3+} ions are shielded from the surface adsorptions. In addition, the cross-relaxation mechanism is dependent of the spatial distance between Er^{3+} and Yb^{3+} ions. In the core–shell NRs, the average distance between Er^{3+} and Yb^{3+} increases due to that the Er^{3+} and Yb^{3+} ions locate in two different layers, leading to the decrease of the cross-relaxation and the relative increase of the green emission. Furthermore, it is obviously to find that the effective energy transfer from Yb^{3+} to Er^{3+} is taken place in the three samples from the Figure 3. In the literatures, the critical separation values of the order of 1.5 nm have been reported for the nonradiative energy transfer for Yb^{3+} and Er^{3+} ions doped in matrices of different nature.[20,21] This means that for separations larger than the critical separation, the probability of nonradiative energy transfer is greatly reduced. In the core–shell NRs, the thickness is about 5 nm, since the probability of nonradiative energy transfer is very low. Nevertheless, the luminescent intensity for CS1 and CS2 is larger than that for the NRs. We suggested that the radiative energy transfer, i.e., reabsorption might be playing an important role.[21]

The variation of the intensity ratio (R_{HS}) of $^2H_{11/2}$–$^4I_{15/2}$ to $^4S_{3/2}$–$^4I_{15/2}$ is closely related to the thermal effect. The energy separation between $^2H_{11/2}$ and $^4S_{3/2}$ is only several hundreds wavenumbers (~700 cm^{-1}). The population distribution between $^2H_{11/2}$ and $^4S_{3/2}$ is dominated by the Bolszmann thermal distribution. This will lead the R_{HS} to be sensitive to temperature. Therefore, R_{HS} is a critical parameter to study the thermal effect in different samples under the exposure of the 978-nm diode laser. Figure 5 shows the intensity ratio of $^2H_{11/2}$–$^4I_{15/2}$ to $^4S_{3/2}$–$^4I_{15/2}$ as a function of excitation power in various samples. It is obviously to observe that the intensity ratio in the core–shell NRs is always smaller than that in the homogeneously doped NRs, even as the Yb^{3+} concentration is higher than that in the core–shell NRs. The larger R_{HS} means the higher local temperature surrounding Er^{3+} ions under the exposure of the 978-nm light. It is not strange

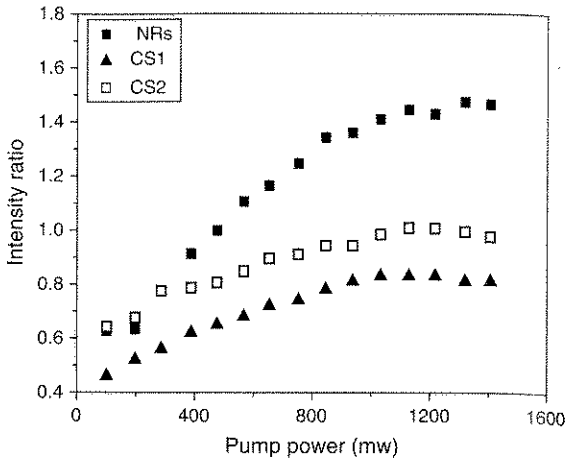

Fig. 5. Intensity ratio of $^2H_{11/2}$–$^4I_{15/2}$ to $^4S_{3/2}$–$^4I_{15/2}$ as a function of excitation power in different samples.

that the local temperature increases with the increase of excitation power and Yb^{3+} concentration. Here, the interesting phenomenon is that in the core–shell NRs the local temperature surrounding luminescent Er^{3+} becomes lower in contrast to the homogeneously codoped powders, suggesting that the thermal effect is avoided to some content. This can be attributed to the thermal "isolation" between Yb^{3+} absorbers and Er^{3+} luminescent centers.

Figures 6(a) and (b) shows the logarithm plots of the emission intensity as a function of excitation power, for

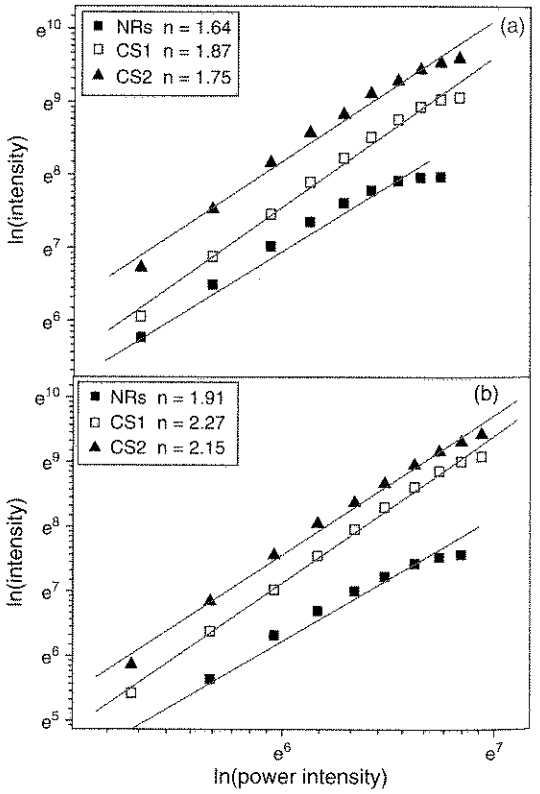

Fig. 6. ln-ln pot of emissions intensity as a function of excitation power in different samples, (a) the red emission, and (b) the green emission.

the green and red emissions in different powders, respectively. The slope (n) in the ln-ln plot increased obviously in the core–shell NRs as shown in the Figure. For the green emission, the values of n were determined to be 1.91, 2.27, and 2.15, respectively, in NRs, CS1, and CS2. For the red, the values of n were determined to be 1.64, 1.87, and 1.75, respectively, in NRs, CS1, and CS2. As is well known, for any upconversion mechanism the visible output power intensity (I_v) will be proportional to some power (n) of the infrared excitation (I_{IR}) power[14, 20]: $I_V \propto I_{IR}^N$, where n is the number of IR phonons absorbed per visible phonon emitted. Generally, the slope for the UCL via a two-photon process approximately equals to 2, however, the previous studies indicate that in Gd_2O_3 NRs the intensity of UCL is proportional to the square of excitation power when the linear decay of the intermediate state is the dominant, while the intensity is proportional to excitation power when the upconversion is the dominant mechanism.[14] The present slope increase in the core–shell NRs may be caused by the decreased ET probability from Yb^{3+} to Er^{3+}, resulting in decreased upconversion relative to the nonlinear decay. On the other hand, the thermal effect may decrease the luminescent intensity as the pumped power high enough, which also causing the decrease of the slopes. In the core–shell NRs, the thermal effect is effective depressed as discussing above, resulting in the larger slopes in CS1 and CS2 comparing to the NRs. The slopes of the red emission are smaller than that of the green emission in all the samples, which can be attributed to the difference of the intermediate level between the green and the red emission. The intermediate level of the green emission is $^4I_{11/2}$, while that of the red emission is $^4I_{13/2}$. On the $^4I_{11/2}$ level, the rate of linear decay is much larger than that on $^4I_{13/2}$ because of efficient nonradiative relaxation of $^4I_{11/2}$–$^4I_{13/2}$.

4. CONCLUSION

In conclusion, $Gd_2O_3:Er^{3+}/Gd_2O_3:Yb^{3+}$ core–shell NRs as well as Er^{3+}, Yb^{3+} homogeneously codoped Gd_2O_3 NRs were synthesized by the hydrothermal method. In the core–shell NRs, due to the decreased cross-relaxation between Er^{3+} and Yb^{3+} ions and the depressed thermal effect caused by the "isolation" of Er^{3+} luminescent centers from Yb^{3+} absorbers, the UCL properties of Er^{3+} ions were considerably improved in contrast to the $Gd_2O_3:Er^{3+}$, Yb^{3+} NRs.

Acknowledgments: This work is supported by the National Nature Science Foundation of China (Grants 10704073, 50772042 and 10504030) and the 863 project of China (2007AA03Z314).

References and Notes

1. S. Lijima, *Nature (London)* 354, 56 (**1991**).
2. V. L. Colvin, M. C. Schlamp, and A. P. Alivisatos, *Nature (London)* 370, 354 (**1994**).
3. V. I. Klimov, A. A. Mikhailovsky, S. Xu, J. A. Hollingsworth, C. A. Leatherdale, H. J. Eisler, and M. G. Bawendi, *Science* 290, 314 (**2000**).
4. B. Dubertret, P. Skourides, D. J. Norris, V. Noireaux, A. H. Brivanlou, and A. Libchaber, *Science* 298, 1759 (**2002**).
5. A. Biswas, G. S. Maciel, R. Kapoor, C. S. Friend, and P. N. Prasad, *Appl. Phys. Lett.* 82, 2389 (**2003**).
6. F. Caruso, M. Spasova, and M. Salgueirno, *Adv. Mater.* 13, 1090 (**2001**).
7. F. Caruso, H. Lichtenfeld, and H. Mohwald, *J. Am. Chem. Soc.* 120, 8523 (**1998**).
8. H. Sertchook and D. Avnir, *Chem. Mater.* 15, 1690 (**2003**).
9. X. Peng, M. C. Schlamp, A. V. Kadavanich, and A. P. Alivisatos, *J. Am. Chem. Soc.* 119, 7019 (**1997**).
10. O. Lehmann, K. Kompe, and M. Haase, *J. Am. Chem. Soc.* 126, 14935 (**2004**).
11. J. W. Stouwdam and F. C. J. M. Van Veggel, *Langmuir* 20, 11763 (**2004**).
12. L. F. Johnson, J. E. Geusic, H. J. Guggenheim, T. Kushida, S. Singh, and L. G. Van Uitert, *Appl. Phys. Lett.* 15, 48 (**1969**).
13. D. C. Hanna, R. M. Percival, and I. R. Perry, *Opt. Commu.* 78, 187 (**1990**).
14. Y. Q. Lei, H. W. Song, L. M. Yang, L. X. Yu, Z. X. Liu, G. H. Pan, X. Bai, and L. B. Fan, *J. Chem. Phys.* 123, 174710 (**2005**).
15. X. Wang and Y. D. Li, *Chem. Eur. J.* 9, 5627 (**2003**).
16. J. Yang, C. X. Li, Z. Y. Cheng, X. M. Zhang, Z. W. Quan, C. M. Zhang, and J. Lin, *J. Phys. Chem. C* 111, 18148 (**2007**).
17. X. Wang and Y. D. Li, Inorg, *Chem.* 45, 7522 (**2006**).
18. C. K. Chang, F. Kimura, T. Kimura, and H. Wada, *Mater. Lett.* 59, 1037 (**2005**).
19. F. Ventrone, C. Boyer, and J. A. Capobianco, *J. Appl. Phys.* 96, 661 (**2004**).
20. L. D. daVila, L. Gomes, L. V. G. Tarelho, S. J. L. Ribeiro, and Y. Messadeq, *J. Appl. Phys.* 93, 3873 (**2003**).
21. A. S. Garcia, R. Serna, M. J. de Castro, and C. N. Afonso, *Appl. Phys. Lett.* 34, 2151 (**2004**).

Received: 25 January 2008. Accepted: 1 June 2008.